Paper 03443

Symposium on
Corrosion Sensor Technologies

DIFFERENTIAL ER-TECHNOLOGY FOR MEASURING DEGREE OF ACCUMULATED CORROSION AS WELL AS INSTANT CORROSION RATE

L.V. Nielsen
MetriCorr ApS
C/O IPL – Materials and Process Technology
Technical University of Denmark, Building 204
DK - 2800 Lyngby, Denmark

K.V. Nielsen
MetriCorr ApS
C/O IPL – Materials and Process Technology
Technical University of Denmark, Building 204
DK - 2800 Lyngby, Denmark

ABSTRACT

A modification of traditional electrical resistance technology is demonstrated which leads to high resolution measurements that can be used to quantify instant corrosion rate in addition to accumulated degree of corrosion. Electrical circuitry, mathematical algorithms, and methods for temperature compensation are demonstrated. The applicability of the technique has been demonstrated in fields where electrochemical techniques are excluded. These include measurements under cathodic polarization and cathodic polarization combined with superimposed alternating currents (AC) as well as measurements of the degradation of electro-galvanized zinc surfaces exposed in salt spray test.

Keywords: High-resolution ER-technology, corrosion rate monitoring, polarization curve, AC induced pipeline corrosion, atmospheric corrosion, electro-deposited zinc.

INTRODUCTION

Measurement of instant corrosion rate is usually made by electrochemical techniques such as linear polarization resistance (LPR), electrochemical impedance spectroscopy (EIS), or electrochemical noise (EN) measurements. Ideally, these techniques provide a measure of corrosion rate within a time period of an hour. Diffusion processes, porous corrosion products and high interfacial capacitance may increase the time constant of the electrochemical reactions that are part of the overall corrosion process, and increase the time to steady state response to potential disturbance. Electrochemical processes occurring parallel to metal dissolution may hide the corrosion processes in resulting measurement leading to incorrect interpretation of

results. Such difficulties are typical when measuring in a range of industrially important environments such as concrete[1], soil[2], district heating waters[3,4], hydrogen sulfide contaminated waters and microbiologically infected environments[5,6]. Further, for some applications the electrochemical techniques are impossible, e.g. under cathodic polarization conditions as well as in the absence of a proper electrolyte such as in atmospheric conditions.

In order to overcome these difficulties, a project on modifying the well known electrical resistance technology was initiated in 1998. The aim of the project was to provide high-resolution ER-technology capable of measuring instant corrosion rate in any environment within an hour, in addition to the traditional measurement of degree of accumulated corrosion.

At present, the modified ER-technology is utilized in several industrial pilot applications. This paper describes principles of the electrical circuitry and experimental verification in terms of results obtained during early laboratory tests. Focus is laid on applicability of the technique under cathodic polarization condition superimposed by alternating current (AC-corrosion), and on atmospheric corrosion monitoring of electro-galvanized zinc exposed in salt spray.

ER-TECHNOLOGY

General Mathematical Algorithms

The ER-technique utilizes the fact that the electrical resistance of a metal probe element increases when corrosion diminishes the thickness of the element. Referring to simple plate geometry for a metal element with dimensions as given in figure 1, the electrical resistance of the element can be expressed by:

$$R = \rho\,(T) \cdot \frac{L}{W \cdot \sigma} \tag{1}$$

where L is length of the element, W is width of the element, and σ is element thickness. The resistivity of the element material $\rho(T)$ can be expressed as:

$$\rho(T) = \rho\,(T_0) \cdot (1+\alpha)^{T-T_0} \tag{2}$$

In this equation, T is temperature, T_0 is the reference temperature, $\rho(T_0)$ is the resistivity of element material at the reference temperature and α is material specific temperature coefficient.

Re-arranging equation (1) gives the thickness of element expressed as a function of element resistance:

$$\sigma = \rho\,(T) \cdot \frac{L}{W} \cdot \frac{1}{R} \tag{3}$$

Differentiation of this equation gives the corrosion rate of the element as:

$$V_{corr} = -\frac{d\sigma}{dt} = \frac{dR}{dt} \cdot \frac{W}{L} \cdot \frac{\sigma^2}{\rho(T)} \tag{4}$$

Hence, if positioned in a corrosive environment, knowledge of the time change of the electrical resistance of the element, the element dimensions, and resistivity of the element material, the corrosion rate can be

quantified. It follows by re-arranging equation (4) that the period of time needed to quantify a certain corrosion rate can be assessed by:

$$\Delta t = \frac{\Delta R}{V_{corr}} \cdot \frac{W}{L} \cdot \frac{\sigma^2}{\rho(T)} \tag{5}$$

The equation predicts that the necessary period of time increase with increasing W/L ratio, and increases with the square of the element thickness. Hence, high sensitivity ER probes can be produced by using thin elements, but this decreases probe lifetime as well. In equation (5), ΔR can be regarded as the minimum resistance change needed to provide a reliable measurement. Improvement of the resolution of the applied ohm-meter then allows for shortening of the necessary period of time needed to quantify a certain corrosion rate without compromising in terms of probe element lifetime.

Circuit Principles

Typically two (or more) metal elements, most often initially identical, are built into an ER probe. One element (denoted hereafter the coupon element, C) is exposed in the hostile environment and diminishes in thickness due to corrosion. The resistance of the coupon element changes primarily with thickness and temperature (according to equations (1) and (2)). A second element (denoted hereafter the reference element, R) is shielded from the hostile environment, e.g. by coating. The resistance of the reference element changes primarily with temperature and the element is used for compensation of this effect.

Figure 2A illustrates traditional ER circuitry. Excitation current is passed through the elements, and amplifiers (A1 and A2) pick up the voltages generated across the elements and scales this properly into a measure of the element resistances, R_C and R_R. Coupon element thickness at time t is then quantified by a mathematical algorithm, for instance:

$$\sigma(t) = \sigma(t=0) \cdot \frac{R_R(t)}{R_C(t)} \cdot \frac{R_C(t=0)}{R_R(t=0)} \tag{6}$$

where (t = 0) refers to initial probe conditions.

Figure 2B illustrates the modified circuitry. Two AC generators provide excitation currents at frequencies f1 and f2. Excitation current is passed from both sides of the elements and returned via grounding in midpoint between the elements. Phase sensitive and frequency selective amplifiers pick up the voltages generated in the circuit. Amplifiers A1 and A2 pick up voltages (f1) across elements C and R respectively, and scale these properly into element resistances (impedances) R_C and R_R. Amplifier A3 picks up directly the difference in voltage (f2) across elements C and R, and scales this properly into differential resistance (impedance) $R_{C\text{-}R}$. Ideally, the initial differential resistance is zero. However, small differences in element dimensions may cause differences in initial element resistances and consequently cause an initial differential resistance different from zero (positive or negative indication). In order to be able to adjust (zero) initial differential resistance, the excitation current (f2) can be supplied/adjusted asymmetrically ($I_C \neq I_R$) to give initial differential voltage equal to zero, and consequently scaled to give an indication of initial differential resistance equal to zero. This facility can be applied at any time throughout a probe lifetime. Measurement of instant corrosion rate is initiated by making the above adjustment. Monitoring the increase in differential resistance over a short period of time provides data for calculation of the instant corrosion rate according to equation (4). The overall scale for the differential resistance measurement is kept within 1-2 mΩ, allowing for a very large magnification as compared with measurement of the absolute value of the element resistance.

Therefore, the period of time needed to quantify a certain corrosion rate (equation (5)) is now diminished by two decades without compromising on probe element lifetime. Instant corrosion rate can now be quantified within (typically and depending on corrosion rate and element designs) half an hour.

EXPERIMENTAL EVIDENCE

Temperature Compensation

Figure 3 shows experimental data for a probe subjected to temperature variations. A probe with carbon steel elements (L = 40 mm, W = 2 mm, σ = 0.1 mm, initial reference element resistance R_R = 21.2 mΩ at 25° C) was exposed in a non-corrosive oil bath. The thermostatically controlled temperature in the oil bath was changed over approximately 8 hours from 25°C to 75°C and the resistance and temperature were recorded on a data logger. Figure 3a shows a very nice correlation between absolute reference element resistance and temperature, showing that the (reference) element resistance is controlled by the temperature. This correlation is the basis for temperature correction in traditional ER-technology. Figure 3b shows differential resistance $R_{C\text{-}R}$ recorded simultaneously in the same temperature interval as a function of the measured absolute reference element resistance. The differential resistance was adjusted to 130 $\mu\Omega$ at 25°C. It can be shown that the differential resistance should act as a true resistance with respect to temperature dependency (equations (1) and (2)). The data in figure 3b show a nice correlation between the reference element resistance (which becomes a measure of the temperature) and the differential resistance. If adjusting the initial differential resistance to a negative value at 25°C, equation (2) predicts negative slope when increasing the temperature. This behavior is experimentally verified by the data illustrated in figure 3c, in which the differential resistance was adjusted to -37 $\mu\Omega$ at 25°C. By adjusting the differential impedance to zero, equation (2) predicts no effect of the temperature increase. Figure 3d shows the experimental data from such experiment. As observed, the facility of adjusting the differential impedance provides a powerful means for temperature compensation.

Polarization Curve and Cathodic Polarization

Figure 4 shows the experimental data for an ER-probe kept under potentiostatic control for 15 minutes at different potentials in 0.5M NaAc/HAc buffer solution (pH = 6, ambient laboratory temperature). The probe elements were made from Armco iron (L/W = 10, σ = 0.025 mm). Electrical connections to the probe element were established by mounting the elements as part of a printed circuit board (PCB). In this manner, simple laboratory probes are readily prepared. The probe was used as the working electrode in a traditional electrochemical cell, with saturated calomel electrode (SCE) as reference, and platinum mesh as a counter electrode. A Wenking type laboratory potentiostat was coupled in the circuit for potential control. The probe was successively polarized at 7 different potentials (-750, -725, -700, -675, -650 (open circuit potential, OCP), -550, and -450 mV SCE) and a data logger recorded the ER data as well as the probe DC current. Figure 4a shows resulting polarization curve compared with corrosion rates obtained by the ER data. Figures 4b, 4c, and 4d illustrate development in the differential resistance for three experimental periods (OCP (-650 mV SCE), -675 mV, and -725 mV SCE). The slope of the resistance increase with time was used to calculate the corrosion rate using equation (4). As observed from these figures, the resistance resolution is in this case well below 0.5 $\mu\Omega$, and the corrosion rates are readily measured within 15 minutes. From figure 4a, it is evident that the correlation with electrochemical data (anodic branch) is quite fine. The corrosion rate at the OCP is well in agreement with extrapolation of the cathodic polarization branch (oxygen reduction). The ER-measurement under cathodic polarization gives plausible suggestions for the corrosion rate – a feature clearly not provided by electrochemical techniques.

AC Induced Corrosion

Figure 5 shows a schematic illustration of the laboratory set-up used to study the influence of superimposed AC on polarization- and corrosion behavior of steel. ER-probes were manufactured and mounted in a standard electrochemical cell as described previously. A 50 Hz AC transformer and a DC scan generator were coupled to the potentiostat control/input terminals in order to provide AC superimposed onto the DC condition. The DC scanner made it possible to perform a slow DC scan and hereby record polarization curves under influence of the superimposed AC. Caused by the superimposed AC, the potential of the working electrode (ER-probe) oscillates between max/min values. In order to make measurements of the true – IR-free – potential oscillation, a Ramlog Correal recorder from a.b.i. data was inserted in the working electrode circuit. This instrument, the functionality of which is described in details by Pourbaix et al[7,8]) disrupts the current for a short period of time (1 ms) and measures the resulting IR free potential. The potential and current data as well as the data from the ER instrumentation were recorded by a data logger

Figure 6 shows data on the effect of superimposed AC on polarization behavior and corrosion rate of steel exposed in an artificial soil solution (5mM Na_2SO_4, 2.5mM $NaHCO_3$, 10mM NaCl – pH = 8.2, conductivity = 2.5 mS/cm). The DC scan rate was 30 mV/h. Figure 6a shows the pure DC condition. A good correlation between the anodic branch of the polarization curve and the corrosion rate measured by the ER-technique is observed. The corrosion rate detected by the ER-instrumentation under mild cathodic polarization seems very plausible. Figures 6b, 6c, and 6d illustrate the effect of superimposed AC (30, 100, and 300 A/m^2) on the polarization- and corrosion behavior. The potential oscillation increases with increasing AC, which causes increasingly severe corrosion conditions even under cathodic polarization. This effect is readily studied by use of the high sensitivity ER-technology. The effect of AC on the corrosion behavior is a concern where pipelines are running parallel to high-voltage power lines[7-11]. High levels of AC can be induced and superimposed onto the DC cathodic protection polarization of the pipe. In Denmark, high sensitivity ER-sensors are now used to monitor the pipeline corrosion conditions[10,11].

Electro-Galvanized Steel in Salt Spray Test

The resistance of a zinc-coated steel plate element (figure 7) can be calculated according to the equation valid for a parallel resistor couple:

$$R_{Total} = \frac{1}{\frac{1}{R_{Fe}} + \frac{1}{R_{Zn}}} \tag{7}$$

where R_{Fe} is the resistance of the steel plate and R_{Zn} is the resistance of the zinc layer. By using equation (1) with respect to the zinc layer and the steel plate and inserting into (7) this resistance can be described as a function of the thickness of the zinc layer σ_{Zn} by:

$$R_{Total}(\sigma_{Zn}) = \frac{R_{Fe} \cdot K}{K + R_{Fe} \cdot \sigma_{Zn}} \quad \text{where } K = \rho_{Zn}(T) \cdot \frac{L}{W} \tag{8}$$

Differentiation gives

$$\frac{dR_{Total}}{d\sigma_{Zn}} = \frac{-R_{Fe}^2 \cdot K}{(K + R_{Fe} \cdot \sigma_{Zn})^2} \tag{9}$$

The corrosion rate of the zinc layer can be expressed as

$$V_{corr} = -\frac{d\sigma_{Zn}}{dt} = \frac{\frac{dR_{Total}}{dt}}{-\frac{dR_{Total}}{d\sigma_{Zn}}} = \frac{dR_{Total}}{dt} \cdot \frac{(K + R_{Fe} \cdot \sigma_{Zn})^2}{R_{Fe}^2 \cdot K} \quad (10)$$

Hence, having knowledge of the thickness and the specific resistance of the zinc layer as well as the thickness and the specific resistance of the steel plate, the corrosion rate of the zinc layer can be measured by measuring the time change of the total resistance.

Figure 8a shows temperature characteristics for the resistance of the individual layers (zinc and steel) as well as the temperature characteristics of the total element resistance. For this experiment, an ER probe was manufactured from a thin steel foil (L = 75 mm, W = 7.5 mm, σ = 0.025 mm). Prior to the zinc plating, the bare steel probe element was exposed in an inert oil bath and the resistance of the element was measured at five different temperatures in the range 20-50°C. These data are presented in figure 8a. Subsequently, the ER probe steel element was electroplated with zinc in a commercial semi-bright acid chloride bath (2A/dm^2 for 17.5 min.). The resulting thickness of the zinc layer (0.01 mm) was measured using x-ray technique. The plated ER probe was again placed in the inert oil bath and the resistance of the coated element was measured at five different temperatures in the range 20-50°C. These data are presented in figure 8a as well. The temperature dependence of the zinc layer resistance was now calculated by re-arranging equation (7) to describe the resistance of the zinc layer as a function of the total resistance and the steel plate resistance. These calculated data for the zinc layer are shown in figure 8a as well. The procedure described above gives the data needed for utilizing equation (10).

Figure 8b shows data from a salt spray test in which the ER probe (manufactured as described above) was exposed under cyclic conditions – 4 hour 30°C salt spray (0.05wt-% NaCl, 0.35wt-% $(NH_4)_2SO_4$, pH 5.0 - 5.4) then 2 hours drying at 40°C. As observed in figure 8b, the ER technique provides means for a real time monitoring of the thickness of the zinc layer. The initial value for the thickness of the layer (9.75 µm) was established by x-ray measurement and used for adjustment of the mathematical equations. 5 cycles (salt spray – dry) were completed in the test. During the drying condition, the ER measurement raw data were problematic to fit into a corrosion scenario and are disregarded at present. However, small reductions in layer thicknesses can be registered after the drying period showing the effect of the concentrated salt solution formed on the surface at some stages when drying the probe. Note as well that x-ray measurement of the layer thickness after the test period was in good agreement with the layer thickness measured by the ER-technique.

The above described procedure has been used to characterize electro-deposited zinc layers with different subsequent treatments (blue chromate passivation, yellow chromate passivation, chromate-free passivation etc.)[12, 13]

CONCLUSIONS

Concepts of the electrical circuitry and the mathematical algorithms for a modified electrical resistance corrosion sensor technique have been presented. It has been demonstrated that the modification involving differential measurement principles improves the resolution by two decades. This high sensitivity ER-measurement can be used to quantify the instant corrosion rate in addition to the accumulated degree of

corrosion resulting from traditional ER-technology. Experimental evidence for the capability of making temperature compensation has been presented. Corrosion rate data obtained by the technique are shown to correlate with electrochemical polarization measurements. Under conditions where electrochemical measurements cannot provide a measure of the corrosion rate, the modified ER-technique seems to be a powerful alternative. This has been demonstrated by measurements under cathodic polarization and cathodic polarization combined with superimposed alternating currents (AC) as well as by measurements of the degradation of electro-galvanized zinc surfaces exposed in salt spray test (atmospheric corrosion conditions).

ACKNOWLEDGEMENTS

ER-technology developed and funded by VN-Instruments ApS. AC corrosion studies funded by National Oil and Gas company of Denmark (DONG A/S). Salt spray tests on electro-galvanized zinc performed by former Ph.D. student F. Fontenay.

REFERENCES

1. K. Videm, Proc. 15th International Corrosion Congress, paper 730, Granada, Spain, ICC, 2002.
2. L.V. Nielsen et al, EFP-95 project, ENS 1313/95, Danish ministry for environment and energy, 1998.
3. S. Richter, Proc. 15th International Corrosion Congress, paper 704, Granada, Spain, ICC, 2002.
4. L.R. Hilbert et al, Proc. 15th International Corrosion Congress, paper 797, Granada, Spain, ICC, 2002.
5. L.R. Hilbert, Monitoring Microbially influenced corrosion, Ph.D. thesis, IPL- Materials Technology, Technical University of Denmark, 2000.
6. L.V. Nielsen and L.R. Hilbert, "Microbial corrosion of steel by sulphate-reducing bacteria: Electrochemical and mechanistic approach", in Aspects of microbially induced corrosion (Ed. D. Thierry), EFC publication no. 22, The Institute of Materials, London, 1997, pp. 11-24.
7. A. Pourbaix et al, Measurement of the importance of AC induced corrosion, Proc. Eurocorr 2000 (Topic 16), London. England , Institute of Materials and EFC, 2000.
8. A. Pourbaix et al, Proc. Eurocorr 2001, paper 228, Riva del Garda, Italy, EFC, 2001
9. F. Stalder et al. AC corrosion on cathodically protected pipelines, Proc. 5th international congress CeoCor, Brussels, Belgium, CeoCor, 2000.
10. L.V. Nielsen, Proc. Eurocorr 2001, paper 20, Riva del Garda, Italy, EFC, 2001.
11. L.V. Nielsen, Proc. 15th International Corrosion Congress, paper 796, Granada, Spain, ICC, 2002
12. F. Fontenay and L.V. Nielsen, "Atmospheric corrosion monitoring of electrolytic zinc coatings by electrical resistance measurements", proc. SUR/FIN 2001, Nashville, USA, 2001
13. F. Fontenay, Process, microstructure and corrosion of electrodeposited zinc, Ph.D. thesis, IPL-Materials Technology, Technical University of Denmark, 2002
14. International patent application, PCT/DK00/00689, VN-Instrument, 2000).

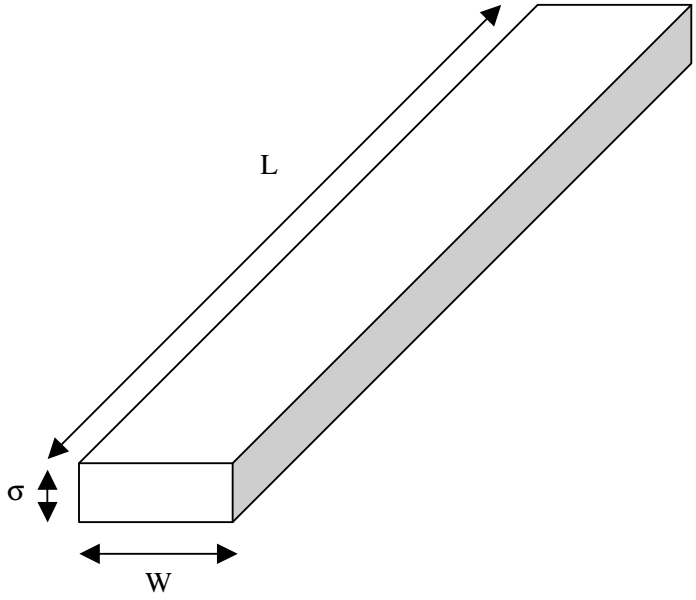

FIGURE 1 - Schematic illustration of simple sensor element.

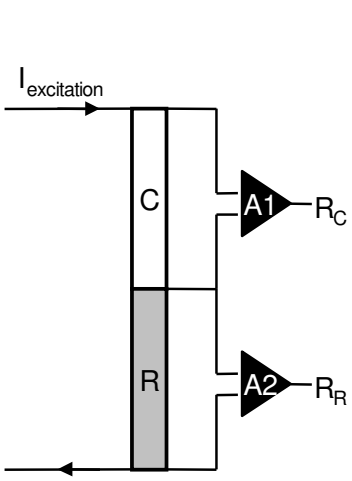

FIGURE 2a – Schematic illustration of traditional excitation circuit.

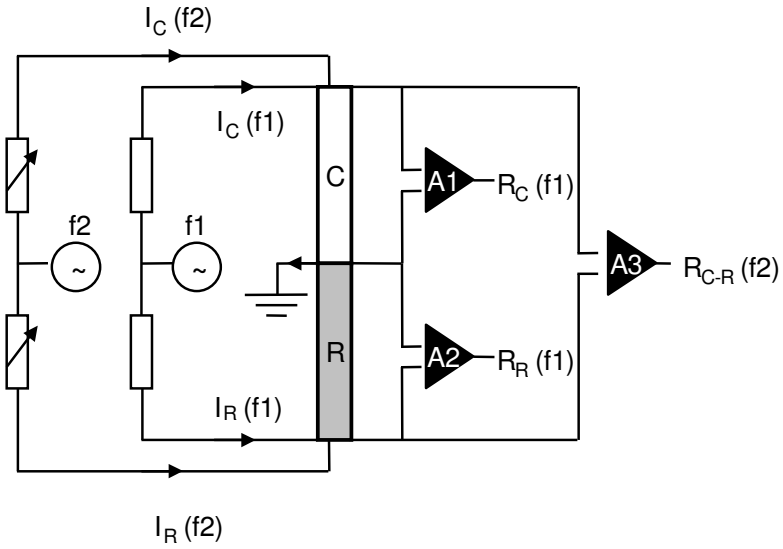

FIGURE 2b – Schematic illustration of modified excitation circuit.

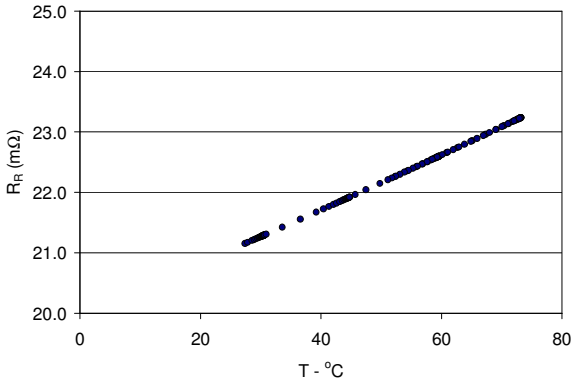

FIGURE 3a – Temperature test, reference element resistance versus temperature.

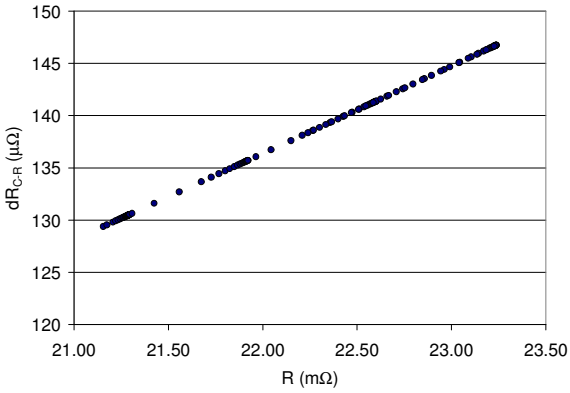

FIGURE 3b – Temperature test, differential resistance (initial adjustment 130 μΩ at 25°C) versus reference resistance.

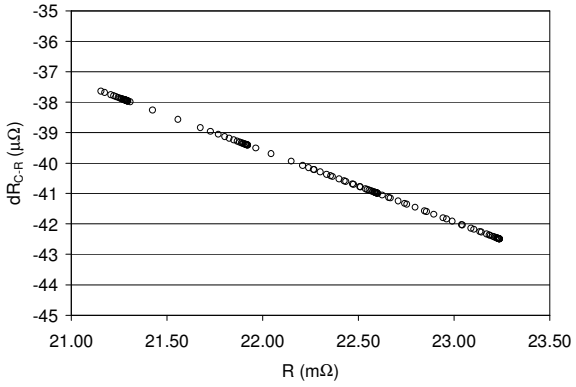

FIGURE 3c - Temperature test, differential resistance (initial adjustment -37 μΩ at 25°C) versus reference resistance.

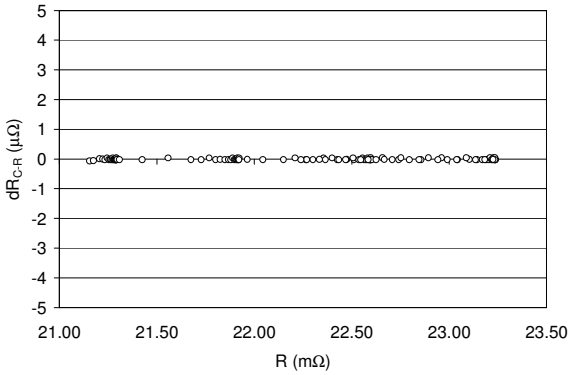

FIGURE 3d - Temperature test, differential resistance (initial adjustment 0 μΩ at 25°C) versus reference resistance.

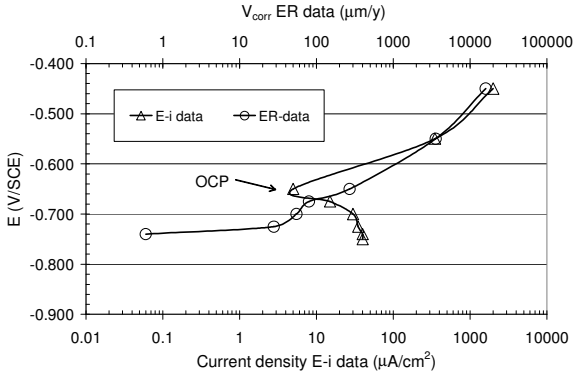

FIGURE 4a – Polarization curve for steel, exposed in HAc/NaAc buffer system and corresponding corrosion rates obtained by the ER data.

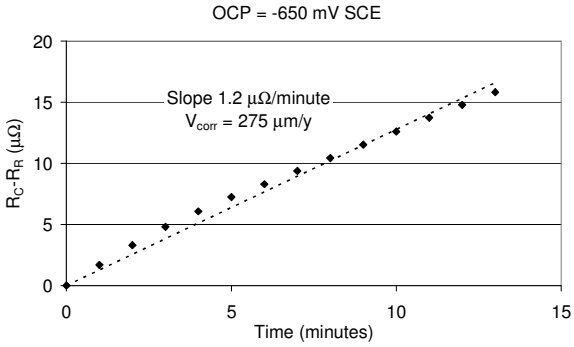

FIGURE 4b – ER data corresponding open circuit conditions in HAc/NaAc buffer system.

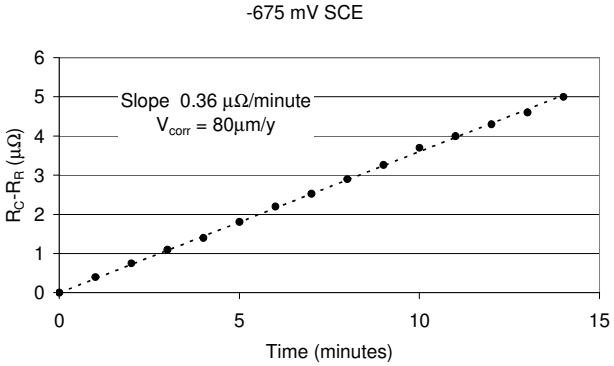

FIGURE 4c - ER data at -675 mV SCE (25 mV cathodic polarization) in HAc/NaAc buffer system.

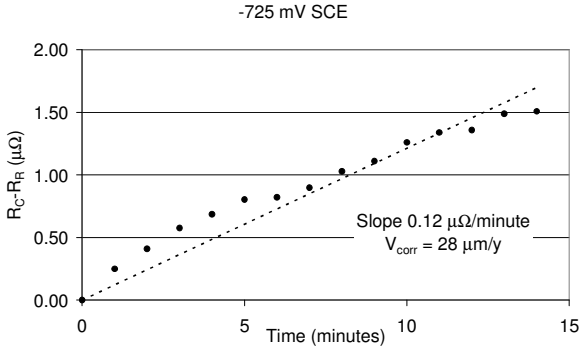

FIGURE 4d - ER data at -725 mV SCE (75 mV cathodic polarization) in HAc/NaAc buffer system.

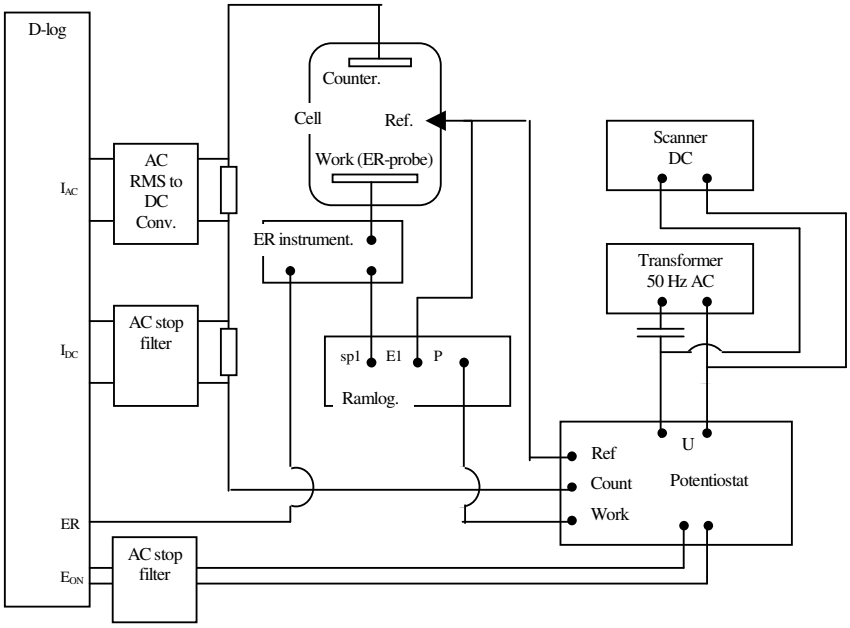

FIGURE 5 - Schematic illustration of laboratory set-up for AC corrosion studies.

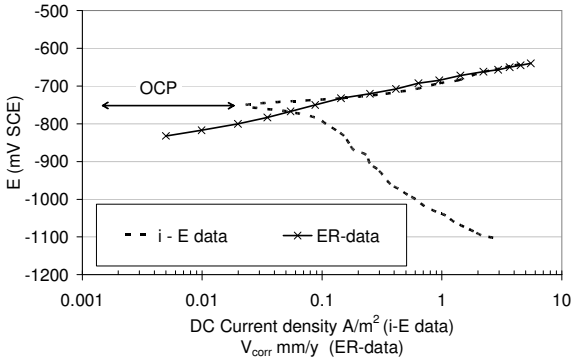

FIGURE 6a – DC polarization behavior and corrosion rate measurement with no superimposed AC in synthetic soil water.

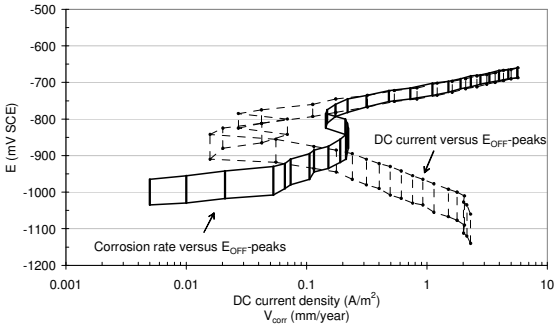

FIGURE 6b – DC polarization behavior and corrosion rate measurement with 30 A/m^2 superimposed AC in synthetic soil water.

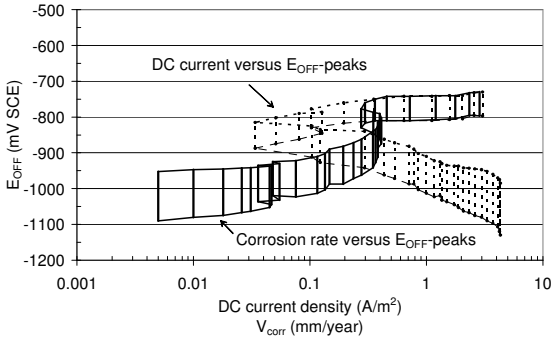

FIGURE 6c – DC polarization behavior and corrosion rate measurement with 100 A/m^2 superimposed AC in synthetic soil water.

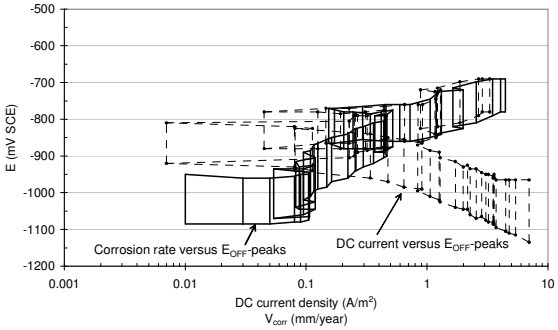

FIGURE 6d – DC polarization behavior and corrosion rate measurement with 300 A/m^2 superimposed AC in synthetic soil water.

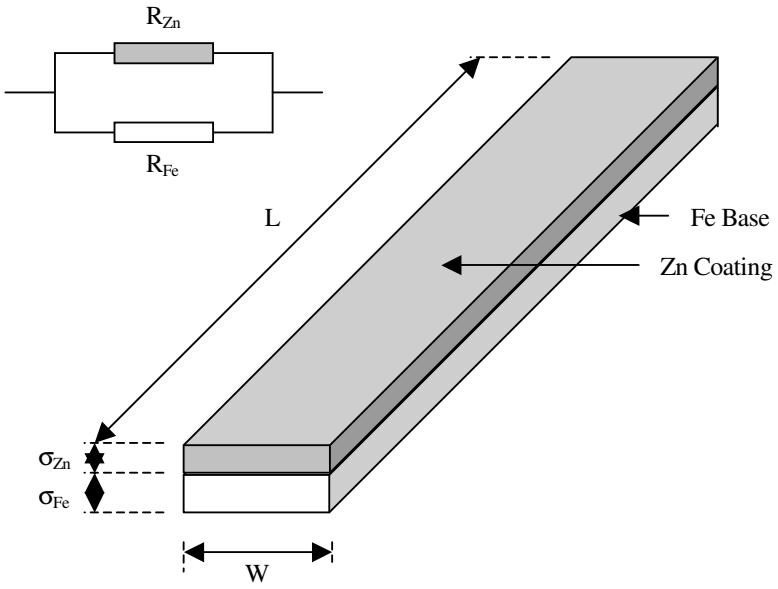

FIGURE 7 – Schematic illustration of sensor element – Fe base coated with Zn.

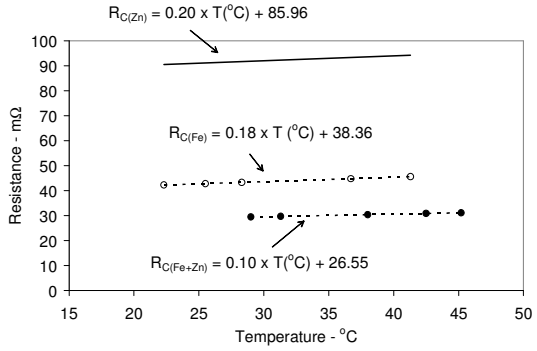

FIGURE 8a – Temperature characteristic of zinc layer resistance, steel plate resistance, and total resistance.

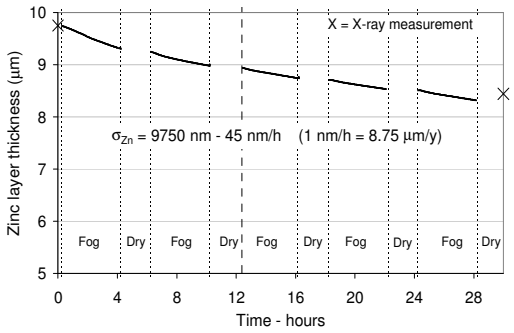

FIGURE 8b – Real time monitoring of degradation of the zinc layer in salt spray test using ER probe.

Figure captions:

FIGURE 1 - Schematic illustration of simple sensor element.

FIGURE 2a – Schematic illustration of traditional excitation circuit.

FIGURE 2b – Schematic illustration of modified excitation circuit.

FIGURE 3a – Temperature test, reference element resistance versus temperature.

FIGURE 3b – Temperature test, differential resistance (initial adjustment 130 μΩ at 25°C) versus reference resistance.

FIGURE 3c - Temperature test, differential resistance (initial adjustment -37 μΩ at 25°C) versus reference resistance.

FIGURE 3d - Temperature test, differential resistance (initial adjustment 0 μΩ at 25°C) versus reference resistance.

FIGURE 4a – Polarization curve for steel, exposed in HAc/NaAc buffer system and corresponding corrosion rates obtained by the ER data.

FIGURE 4b – ER data corresponding open circuit conditions in HAc/NaAc buffer system.

FIGURE 4c - ER data at -675 mV SCE (25 mV cathodic polarization) in HAc/NaAc buffer system.

FIGURE 4d - ER data at -725 mV SCE (75 mV cathodic polarization) in HAc/NaAc buffer system.

FIGURE 5 - Schematic illustration of laboratory set-up for AC corrosion studies.

FIGURE 6a – DC polarization behavior and corrosion rate measurement with no superimposed AC in synthetic soil water.

FIGURE 6b – DC polarization behavior and corrosion rate measurement with 30 A/m^2 superimposed AC in synthetic soil water.

FIGURE 6c – DC polarization behavior and corrosion rate measurement with 100 A/m^2 superimposed AC in synthetic soil water.

FIGURE 6d – DC polarization behavior and corrosion rate measurement with 300 A/m^2 superimposed AC in synthetic soil water.

FIGURE 7 – Schematic illustration of sensor element – Fe base coated with Zn.

FIGURE 8a – Temperature characteristic of zinc layer resistance, steel plate resistance, and total resistance.

FIGURE 8b – Real time monitoring of degradation of the zinc layer in salt spray test using ER probe.